Linear electro-optic effect in semiconductors: *Ab initio* description of the electronic contribution

Lucie Prussel and Valérie Véniard*
Laboratoire des Solides Irradiés, École Polytechnique, CNRS, CEA/DRF, 91128 Palaiseau, France and European Theoretical Spectroscopy Facility (ETSF)

(Received 3 January 2018; revised manuscript received 11 April 2018; published 1 May 2018)

We propose an *ab initio* framework to derive the electronic part of the second-order susceptibility tensor for the electro-optic effect in bulk semiconductors. We find a general expression for $\chi^{(2)}$ evaluated within time-dependent density-functional theory, including explicitly the band-gap corrections at the level of the scissors approximation. Excitonic effects are accounted for, on the basis of a simple scalar approximation. We apply our formalism to the computation of the electro-optic susceptibilities for several semiconductors, such as GaAs, GaN, and SiC. Taking into account the ionic contribution according to the Faust-Henry coefficient, we obtain a good agreement with experimental results. Finally, using different types of strain to break centrosymmetry, we show that high electro-optic coefficients can be obtained in bulk silicon for a large range of frequencies.

DOI: 10.1103/PhysRevB.97.205201

I. INTRODUCTION

A deep understanding of the nonlinear optical properties of solids is crucial for the improvement of nonlinear devices and provides an opportunity to search for new materials. Among all the nonlinear phenomena existing in nature, an important role is played by the electro-optic effect. The electro-optic effect produces a change of the refractive index in a medium using a dc electric field. In the linear electro-optic effect (LEO) or Pockels effect, the change is proportional to the applied electric field. It may be seen as a second-order polarization and then described by a second-order susceptibility, which is known to be zero in the dipole approximation for centrosymmetric materials. Therefore a peculiarity of the LEO effect comes from the fact that it only occurs in materials without inversion symmetry or originates from symmetry-breaking regions.

LEO has attracted particular interest for the development of optoelectronic devices. Experimental efforts are made toward the design, fabrication, and search for nonlinear optical materials. In particular, it has been established that electrorefractive effect is a promising route to realize efficient high speed optical modulators [1]. Recently, a giant electro-optic effect has been observed in Ge/SiGe coupled quantum wells which can be exploited to enhance the performance of optical modulators [2]. On the other hand, noncentrosymmetry in crystals can be obtained by applying an asymmetric strain. It has been reported that strain in a Si photonic crystal waveguide induces strong nonlinearities and enables electro-optic effects, showing that data processing and transmission could be potentially performed by all-silicon components [3,4]. Moreover, among recent applications of the LEO effects, one can cite the possibility of achieving quasiperfect phase matching conditions in homogeneous crystals, based on controllable birefringence via the linear electro-optic effect [5]. Finally, because of its sensitivity to space symmetry, LEO can be used as a sensitive, nondestructive and noninvasive probe for studying many kinds of surfaces and interfaces in semiconductors [6,7].

The design of optimized devices and the search for new electro-optic materials requires accurate values for the second-order susceptibilities. The experimental characterization is not an easy task and requires high-quality crystals. From the theoretical point of view, most of the calculations for second-order susceptibilities have been done in the framework of second-harmonic generation (SHG) (see, for instance, Ref. [8], and references therein). In that case, the frequency of the incoming field is considered as high with respect to vibrational frequencies and the lattice is kept static. Therefore, one has to evaluate only the electronic contribution, obtained directly from the optical susceptibility, coming from the interaction of the valence electrons and the electric fields. The knowledge of the electro-optic tensor implies, in principle, the evaluation of two additional contributions, i.e., the ionic and piezoelectric parts. The ionic contribution is linked to the ionic displacements and depends on the variation of the dielectric tensor induced by these displacements. The sum of the electronic and ionic contributions is usually referred to as the clamped value. The piezoelectric contribution comes from the possible modification of the shape of the unit cell due to the electric forces and leads to the so-called unclamped value. For more details, see Refs. [9,10].

The theoretical description of the second-order response is a difficult task and only a small number of *ab initio* works exist on the topic, mainly focused on the SHG response. In the first theoretical works on LEO, Hughes and Sipe presented a first-principles calculation of the susceptibility in crystals based on the independent-particle approximation, where self-energy effects were included at the level of a scissors operator [11]. However, it was pointed out later, by some of the authors, that unlike the case of linear optics the inclusion of the scissors operator in the nonlinear susceptibilities was far from being a rigid shift and that it had to be treated with special care [12]. Since then the effect of the scissor operator has been carefully

*Corresponding author: valerie.veniard@polytechnique.fr

 ©2018 American Physical Society

analyzed for SHG but has not been investigated for LEO. A different approach from the sum over states methods cited above was presented by Veithen *et al.* for the static susceptibility in a formalism based on the Berry phase and applied to ferroelectric oxides [9,10,13] and Zn compounds [14].

In the following, we will show our results for the second-order susceptibility describing the LEO tensor, within the *ab initio* framework of time-dependent density-functional theory (TDDFT). The paper is organized as follows: In Sec. II, we present our analytic derivation of the macroscopic polarization up to second order in terms of the electric fields, including the effect of a scissors operator to account for the quasiparticle effect. Excitonic effects will be included on the basis of a simple approach. The results for second-harmonic generation will be shown for comparison. In Sec. III, we illustrate the validity of our formalism with the calculation of $\chi^{(2)}$ for several semiconductors in a large frequency range and for different light-polarization directions. These results will be compared to experimental data when available. Finally we will address the case of strained silicon.

II. FORMALISM AND METHODS

The macroscopic second-order polarization, at frequency ω, in terms of the time-dependent electric field $\mathbf{E}(\omega)$ and the static field $\mathbf{E}$ is expressed in frequency space as

$$\mathbf{P}^{(2)}(\omega) = 2\,\chi^{(2)}(-\omega;\omega,0) : \mathbf{E}(\omega)\,\mathbf{E}. \tag{1}$$

The factor 2 in front of the susceptibility appears when the two input frequencies are different, i.e., for the sum- or difference-frequency generation (see Appendix A of Ref. [11] for more details). In the independent-particle approximation (IPA) the rank-3 tensor $\chi^{(2)}(-\omega;\omega,0)$ is connected to the second-order response function $\chi_0^{(2)}(\mathbf{q},\mathbf{q}_1,\mathbf{q}_2,\omega_1,\omega_2)$, expressed as (atomic units will be used unless otherwise stated; $\hbar = 1, e = 1, m = 1$)

$$\chi_0^{(2)}(\mathbf{q},\mathbf{q}_1,\mathbf{q}_2,\omega_1,\omega_2) = \frac{2}{V}\sum_{n,m,p}\sum_{\mathbf{k}} \frac{\langle\phi_{n,\mathbf{k}}|e^{-i\mathbf{qr}}|\phi_{m,\mathbf{k+q}}\rangle\langle\phi_{m,\mathbf{k+q}}|e^{i\mathbf{q}_1\mathbf{r}_1}|\phi_{p,\mathbf{k+q}_2}\rangle\langle\phi_{p,\mathbf{k+q}_2}|e^{i\mathbf{q}_2\mathbf{r}_2}|\phi_{n,\mathbf{k}}\rangle}{E_{n,\mathbf{k}} - E_{m,\mathbf{k+q}} + \omega_1 + \omega_2 + 2i\eta}$$
$$\times\left(\frac{f_{n,\mathbf{k}} - f_{p,\mathbf{k+q}_2}}{E_{n,\mathbf{k}} - E_{p,\mathbf{k+q}_2} + \omega_2 + i\eta} + \frac{f_{m,\mathbf{k+q}} - f_{p,\mathbf{k+q}_2}}{E_{p,\mathbf{k+q}_2} - E_{m,\mathbf{k+q}} + \omega_1 + i\eta}\right) + [(\mathbf{q}_1,\omega_1) \leftrightarrow (\mathbf{q}_2,\omega_2)], \tag{2}$$

where the vectors $\mathbf{q}_1$ and $\mathbf{q}_2$ are along the polarization of the electric fields and $\mathbf{q} = \mathbf{q}_1 + \mathbf{q}_2$, $\phi_{n,\mathbf{k}}$ denotes the Bloch wave functions, the wave vector $\mathbf{k}$ lies in the first Brillouin zone, with a normalization volume V, and $f_{n,\mathbf{k}}$ are Fermi occupation numbers, which are considered to be either 0 or 1 for unoccupied and occupied states, respectively. The spin is accounted for by a factor 2 in the above expression. This IPA response function is then related to the second-order susceptibility by the following equation:

$$\hat{\mathbf{q}}\,\overset{\leftrightarrow}{\chi}^{(2)}(\omega_1,\omega_2)\,\hat{\mathbf{q}}_1\,\hat{\mathbf{q}}_2 = -\frac{i}{2}\,\chi_0^{(2)}(\hat{\mathbf{q}},\hat{\mathbf{q}}_1,\hat{\mathbf{q}}_2,\omega_1,\omega_2). \tag{3}$$

As we are interested in the low-energy part of the spectrum, we consider only the optical limit ($q \to 0$). We have used the $\mathbf{k}\cdot\mathbf{p}$ perturbation theory and followed the derivation of Ref. [15] to expand Eq. (2).

In principle, electron bands have to be calculated within the many-body formalism, using the GW approach. However, its application is not trivial in the calculation of second-order response functions and we have used instead a simpler approach, the so-called scissors operator [12],

$$\hat{S} = \Sigma_s \sum_{\mathbf{k}}\sum_{n}(1 - f_{n,\mathbf{k}})|\phi_{n,\mathbf{k}}\rangle\langle\phi_{n,\mathbf{k}}|, \tag{4}$$

accounting for the GW gap corrections

$$E^{\Sigma}_{n,\mathbf{k}} = E_{n,\mathbf{k}} + (1 - f_{n,\mathbf{k}})\Sigma_s. \tag{5}$$

The scissors operator is nonlocal and has to be treated with special care when performing the $\mathbf{k}\cdot\mathbf{p}$ expansion, as it does not commute with the position operator. After some lengthy calculations, the second-order susceptibility contains two contributions: a two-band term

$$\chi_0^{(2),2bnd}(\hat{\mathbf{q}},\hat{\mathbf{q}}_1,\hat{\mathbf{q}}_2,\omega,0) = \frac{2}{V}\sum_{\mathbf{k}}\sum_{n,m}\frac{f_{nm}}{(E^{\Sigma}_{nm,\mathbf{k}} + \tilde{\omega})}[\Delta_{nm,\mathbf{k}}(\hat{\mathbf{q}}_1)\hat{\mathbf{r}}_{nm,\mathbf{k}}(\hat{\mathbf{q}}_2)\hat{\mathbf{r}}_{mn,\mathbf{k}}(\hat{\mathbf{q}})$$
$$+ \Delta_{nm,\mathbf{k}}(\hat{\mathbf{q}})\hat{\mathbf{r}}_{nm,\mathbf{k}}(\hat{\mathbf{q}}_2)\hat{\mathbf{r}}_{mn,\mathbf{k}}(\hat{\mathbf{q}}_1)]\left(\frac{1}{(E^{\Sigma}_{nm,\mathbf{k}})^2} + \frac{1}{E^{\Sigma}_{nm,\mathbf{k}}\,E_{nm,\mathbf{k}}} - \frac{2}{(E_{nm,\mathbf{k}})^2}\right), \tag{6}$$

and a three-band term, which can be split into interband transitions and intraband transitions:

$$\chi_0^{(2),\text{inter}}(\hat{\mathbf{q}},\hat{\mathbf{q}}_1,\hat{\mathbf{q}}_2,\omega,0) = \frac{2}{V}\sum_{\mathbf{k}}\sum_{n,m,p}\frac{\sigma_{n,m,p}}{(E^{\Sigma}_{nm,\mathbf{k}} + \tilde{\omega})}\left\{\hat{\mathbf{r}}_{nm,\mathbf{k}}(\hat{\mathbf{q}})\hat{\mathbf{r}}_{mp,\mathbf{k}}(\hat{\mathbf{q}}_1)\hat{\mathbf{r}}_{pn,\mathbf{k}}(\hat{\mathbf{q}}_2)\left[-\frac{f_{np}}{E^{\Sigma}_{np,\mathbf{k}}} - \frac{f_{mp}}{(E^{\Sigma}_{pm,\mathbf{k}} + \tilde{\omega})}\right]\right.$$
$$\left. + \hat{\mathbf{r}}_{nm,\mathbf{k}}(\hat{\mathbf{q}})\hat{\mathbf{r}}_{mp,\mathbf{k}}(\hat{\mathbf{q}}_2)\hat{\mathbf{r}}_{pn,\mathbf{k}}(\hat{\mathbf{q}}_1)\left[-\frac{f_{np}}{(E^{\Sigma}_{np,\mathbf{k}} + \tilde{\omega})} - \frac{f_{mp}}{E^{\Sigma}_{pm,\mathbf{k}}}\right]\right\}, \tag{7}$$

$$\chi_0^{(2),\text{intra}}(\hat{\mathbf{q}},\hat{\mathbf{q}}_1,\hat{\mathbf{q}}_2,\omega,0) = \frac{2}{V}\sum_{\mathbf{k}}\sum_{n,m,p}\sigma_{n,m,p}\Bigg\{\hat{\mathbf{r}}_{nm,\mathbf{k}}(\hat{\mathbf{q}})\hat{\mathbf{r}}_{mp,\mathbf{k}}(\hat{\mathbf{q}}_1)\hat{\mathbf{r}}_{pn,\mathbf{k}}(\hat{\mathbf{q}}_2)\Bigg[-\frac{f_{nm}E_{pm,\mathbf{k}}}{2(E^{\Sigma}_{nm,\mathbf{k}}+\tilde{\omega})^2E_{nm,\mathbf{k}}} + \frac{f_{mp}E_{nm,\mathbf{k}}}{2(E^{\Sigma}_{pm,\mathbf{k}}+\tilde{\omega})^2E_{pm,\mathbf{k}}} + \frac{f_{np}(E_{pm,\mathbf{k}}+E_{nm,\mathbf{k}})}{2(E^{\Sigma}_{np,\mathbf{k}}+\tilde{\omega})(E_{np,\mathbf{k}})^2} + \frac{f_{mp}E_{np,\mathbf{k}}}{(E^{\Sigma}_{pm,\mathbf{k}}+\tilde{\omega})E_{pm,\mathbf{k}}}\left(\frac{1}{E^{\Sigma}_{pm,\mathbf{k}}}-\frac{1}{2E_{pm,\mathbf{k}}}\right) + \frac{f_{nm}E_{np,\mathbf{k}}}{(E^{\Sigma}_{nm,\mathbf{k}}+\tilde{\omega})E_{nm,\mathbf{k}}}\left(\frac{1}{E^{\Sigma}_{nm,\mathbf{k}}}-\frac{1}{2E_{nm,\mathbf{k}}}\right)\Bigg] + \hat{\mathbf{r}}_{nm,\mathbf{k}}(\hat{\mathbf{q}})\hat{\mathbf{r}}_{mp,\mathbf{k}}(\hat{\mathbf{q}}_2)\hat{\mathbf{r}}_{pn,\mathbf{k}}(\hat{\mathbf{q}}_1)\Bigg[\frac{f_{nm}E_{np,\mathbf{k}}}{2(E^{\Sigma}_{nm,\mathbf{k}}+\tilde{\omega})^2E_{nm,\mathbf{k}}} + \frac{f_{np}E_{nm,\mathbf{k}}}{2(E^{\Sigma}_{np,\mathbf{k}}+\tilde{\omega})^2E_{np,\mathbf{k}}} + \frac{f_{np}E_{pm,\mathbf{k}}}{(E^{\Sigma}_{np,\mathbf{k}}+\tilde{\omega})E_{np,\mathbf{k}}}\left(\frac{1}{E^{\Sigma}_{np,\mathbf{k}}}-\frac{1}{2E_{np,\mathbf{k}}}\right) - \frac{f_{nm}E_{pm,\mathbf{k}}}{(E^{\Sigma}_{nm,\mathbf{k}}+\tilde{\omega})E_{nm,\mathbf{k}}}\left(\frac{1}{E^{\Sigma}_{nm,\mathbf{k}}}-\frac{1}{2E_{nm,\mathbf{k}}}\right) + \frac{f_{mp}(E_{np,\mathbf{k}}+E_{nm,\mathbf{k}})}{2(E^{\Sigma}_{pm,\mathbf{k}}+\tilde{\omega})(E_{pm,\mathbf{k}})^2}\Bigg]\Bigg\}, \quad (8)$$

where $\sigma_{n,m,p} = 1$ if n, m, and p are all different and $\sigma_{n,m,p} = 0$ otherwise and we have used the following notations:

$$E_{nm,\mathbf{k}} = E_{n,\mathbf{k}} - E_{m,\mathbf{k}}, \qquad \tilde{\omega} = \omega + i\eta. \quad (9)$$

For a clean cold semiconductor, the Fermi occupation numbers do not depend on the wave vector $\mathbf{k}$ and we note $f_{nm} = f_n - f_m$. The operator $\hat{\mathbf{r}}$ is defined in terms of the usual position operator $\mathbf{r}$:

$$\hat{\mathbf{r}}_{nm,\mathbf{k}}(\hat{\mathbf{q}}) = \langle\phi_{n,\mathbf{k}}|i\hat{\mathbf{q}}\hat{\mathbf{r}}|\phi_{m,\mathbf{k}}\rangle \quad \text{if} \quad E_{n,\mathbf{k}} \neq E_{m,\mathbf{k}}$$
$$= 0 \quad \text{if} \quad E_{n,\mathbf{k}} = E_{m,\mathbf{k}}$$

and $\Delta_{nm,\mathbf{k}}(\hat{\mathbf{q}})$ stands for

$$\Delta_{nm,\mathbf{k}}(\hat{\mathbf{q}}) = \hat{\mathbf{v}}_{nn,\mathbf{k}}(\hat{\mathbf{q}}) - \hat{\mathbf{v}}_{mm,\mathbf{k}}(\hat{\mathbf{q}}), \quad (10)$$

where $\mathbf{v}$ is the velocity operator. In practice, the matrix element of $\mathbf{r}$ is calculated in terms of the matrix element of $\mathbf{v}$, with

$$\langle\phi_{n,\mathbf{k}}|i\hat{\mathbf{r}}|\phi_{m,\mathbf{k}}\rangle = \frac{\langle\phi_{n,\mathbf{k}}|\hat{\mathbf{v}}|\phi_{m,\mathbf{k}}\rangle}{E_{n,\mathbf{k}} - E_{m,\mathbf{k}}}. \quad (11)$$

Note that if no scissors correction is applied, the shifted and nonshifted energies, $E^{\Sigma}_{n,\mathbf{k}}$ and $E_{n,\mathbf{k}}$, become equal and we can show that the two-band term is identically zero. This contrasts with the case of second-harmonic generation, in which this term vanishes only for specific cases, such as the cubic symmetry for instance [16].

IPA is the simplest level of approximation for the calculation of the response function and a more accurate description requires the inclusion of many-body effects, i.e., local field and excitonic effects, corresponding to the microscopic fields induced inside the material by the perturbation and to the interaction of electron-hole pairs, respectively (see Ref. [17]). They can be included in the framework of TDDFT through a Dyson equation (see Ref. [15] for details on this calculation in the case of second-harmonic generation). It has been shown for SHG that for some specific materials, such as those presenting the zinc-blende structure, local fields can be neglected while excitonic effects are important [15,18]. Since accounting for the local fields is quite cumbersome, it is interesting for these materials to simplify the Dyson equation and include only the excitonic effects, using the so-called scalar long-range kernel $-\alpha/q^2$, defined in Refs. [19,20] and successfully applied for SHG in Ref. [15].

To account only for the excitonic effects, we will solve a second-order Dyson equation, where the microscopic components of the Coulomb potential have been neglected, retaining only its macroscopic part corresponding to $v(\mathbf{G}=0)$. Therefore, the second-order Dyson equation reduces to a simple scalar equation:

$$\chi^{(2)}(\mathbf{q},\mathbf{q}_1,\mathbf{q}_2,\omega_1,\omega_2) = \chi_0^{(2)}(\mathbf{q},\mathbf{q}_1,\mathbf{q}_2,\omega_1,\omega_2)\left[1+\frac{\alpha}{q_1^2}\chi^{(1)}(\mathbf{q}_1,\omega_1)\right] \times\left[1+\frac{\alpha}{q_2^2}\chi^{(1)}(\mathbf{q}_2,\omega_2)\right] + \chi_0^{(1)}(\mathbf{q},\omega)\,\frac{\alpha}{q^2}\chi^{(2)}(\mathbf{q},\mathbf{q}_1,\mathbf{q}_2,\omega_1,\omega_2), \quad (12)$$

where $\chi_0^{(2)}$ is the IPA response function while $\chi^{(2)}$ includes the excitonic effects and should replace $\chi_0^{(2)}$ in Eq. (3). $\chi^{(1)}$ and $\chi_0^{(1)}$ are the corresponding first-order response functions.

A. Computational details

We first determine the electronic structure of the material in its ground state within density-functional theory (DFT) with the ABINIT package [21–24]. The Kohn-Sham energies and wave functions are obtained in terms of a basis of plane waves. The local density approximation for the exchange-correlation potential is used, with norm-conserving pseudopotentials. The calculation of the nonlinear optical spectra for LEO has been implemented in the 2light code [25].

The converged parameters for all the different compounds are reported in Table I, which includes the cutoff energy E_{cutoff}, the lattice constant a_{cell}, the numbers of off-symmetry shifted k points n_{kpt}, and unoccupied states $n^{\text{unoc}}_{\text{band}}$, as well as the value of the shift Σ_s for the scissors operator in Eq. (4).

B. Comparison between the LEO and SHG susceptibilities

We have first tested our approach on a simple semiconductor, namely, cubic silicon carbide, which is a

TABLE I. Convergence parameters.

	3C-SiC	2H-SiC	GaAs	α-GaN	Si[1]
E_{cutoff} (Ha)	40	40	50	50	20
a_{cell} (Å)	4.36	$a = 3.16$, $c = 5.19$	5.63	$a = 3.19$, $c = 5.17$	5.41
n_{kpt}	4096	18750	27000	6358	16250
$n_{\text{band}}^{\text{unoc}}$	16	22	36	22	44
Σ_s (eV)	0.84	0.8	0.85	1.4	0.6

[1]Strained silicon: the lattice parameters and the atomic positions vary depending on the strain and are given in Sec. III B.

noncentrosymmetric material, with only one nonvanishing component for the second-order susceptibility tensor, $\chi^{(2)}_{xyz}$.

If one considers the limit $\omega \to 0$, the LEO and SHG susceptibilities become equivalent:

$$\lim_{\omega\to 0} \chi^{(2)}_{\text{SHG}}(-2\omega;\omega,\omega) = \lim_{\omega\to 0} \chi^{(2)}_{\text{LEO}}(-\omega;\omega,0), \tag{13}$$

as illustrated in Fig. 1. The factor 2 that usually appears between SHG and SFG susceptibilities is here not included in the definition of the LEO susceptibility but is taken into account in the polarization [see Eq. (1)]. Note that at lower frequencies the SHG curve is rising faster than the LEO one. This can be expected as the first set of resonances starts at half the gap for the SHG process, while only one set of resonances is present for LEO at $\omega > E_{\text{gap}}$.

C. Effect of the scissors correction

To go beyond the independent-particle approximation, we have included a scissors correction [12], for 3C-SiC and one of the hexagonal polytypes 2H-SiC. The correction Σ_s is reported in Table I for both compounds. This kind of calculation will be referred to as the quasiparticle approximation (QPA).

The effect of the scissors on second-order susceptibilities, SHG and LEO, is shown in Fig. 2. It is known that, for the linear response, this effect corresponds to a rigid blue shift of the spectrum, while for the second-harmonic spectrum the peaks are also blue shifted, but the weight of the various contributions is modified [26–28]. The latter has been attributed to the fact that two types

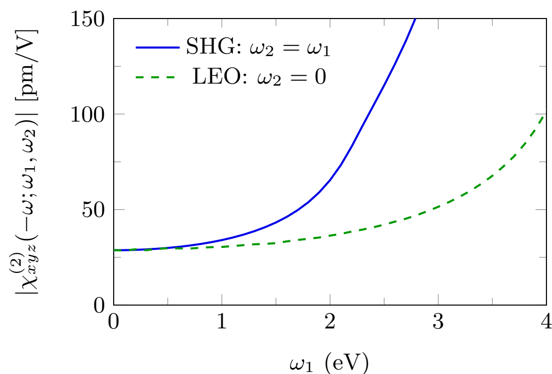

FIG. 1. Comparison between second-order optical responses in 3C-SiC below the band gap: xyz component of the LEO tensor $|\chi^{(2)}_{xyz}(-\omega;\omega,0)|$ (dashed green line) and SHG susceptibility $|\chi^{(2)}_{xyz}(-2\omega;\omega,\omega)|$ (solid blue line).

of denominators, containing $(E_{nm,\mathbf{k}} + 2\omega)$ and $(E_{nm,\mathbf{k}} + \omega)$, appear in the SHG expression of $\chi^{(2)}_{xyz}(-2\omega;\omega,\omega)$. It turns out that in the LEO spectra, only a rigid shift is visible, as displayed in the second row of Fig. 2. The effect of the scissors operator is very similar to the linear case, despite the fact that all eigenvalues $E_{n,\mathbf{k}}$ are not simply replaced by scissored ones $E^{\Sigma}_{n,\mathbf{k}}$. This was also verified for other materials, such as other types of SiC polytypes, GaAs, as well as SiGe superlattices and strained Si which both present a tetragonal symmetry.

III. RESULTS

A. Comparison with experiments

The linear electro-optic effect can be seen as a correction to the dielectric tensor induced by the dc electric field $\mathbf{E}$:

$$\tilde{\varepsilon}_{ij}(\omega) = \varepsilon_{ij}(\omega) + \sum_k 8\pi\ \chi^{(2)}_{ijk}(-\omega;\omega,0)\mathcal{E}_k, \tag{14}$$

where $\mathcal{E}_k$ is the component of the dc field along k. Experimentally, the quantity measured is an electro-optic coefficient $r_{ijk}(\omega)$, defined in terms of the impermeability tensor $\eta_{ij}(\omega)$ and corresponding to the inverse of the permittivity $\varepsilon_{ij}(\omega)$:

$$\tilde{\eta}_{ij}(\omega) = \eta_{ij}(\omega) + r_{ijk}(\omega)\mathcal{E}_k. \tag{15}$$

It is linked to the second-order susceptibility by the relation

$$\chi^{(2)}_{ijk}(-\omega;\omega,0) = -\frac{1}{8\pi}\ n_i^2(\omega)n_j^2(\omega)r_{ijk}(\omega). \tag{16}$$

1. Gallium arsenide

Previous LEO numerical results were published by Hughes and Sipe [11] and applied to GaAs and GaP, yielding a good agreement with experimental results. However, a decade later, it was shown by the same authors (Ref. [12]) that the scissors correction was incorrectly implemented in nonlinear calculations. A new implementation was proposed for SHG and the comparison among the two calculations for GaAs shows that there is a difference close to a factor 2 at low energy. It is expected that such a difference remains for LEO in this energy range, since the susceptibilities for SHG and LEO become equivalent at zero frequency [see Eq. (13)]. The good agreement with experiments that was observed, despite the old implementation of the scissors operator, is explained by the fact that the comparison was performed with the full clamped electro-optic coefficients r^S_{ijk} measured experimentally, whereas only the electronic contribution was included in the calculation. While only considering the electronic part may be a good approximation for SHG since the phonons only become significant when the input frequency drops below 10^{-2} eV [29], it is not enough for LEO which is generated by a static field, and therefore may contain a non-negligible ionic part due to phonons.

The total electro-optic coefficient, also called the unclamped or *stress-free* LEO coefficient, is expressed as

$$r^T_{ijk} = r^S_{ijk} + r^P_{ijk} = r^{S,e}_{ijk} + r^{S,i}_{ijk} + r^P_{ijk}, \tag{17}$$

where r^S_{ijk} is called the clamped or strain-free LEO coefficient and r^P_{ijk} represent the inverse piezoelectric contribution. The clamped coefficient itself can be separated into an electronic

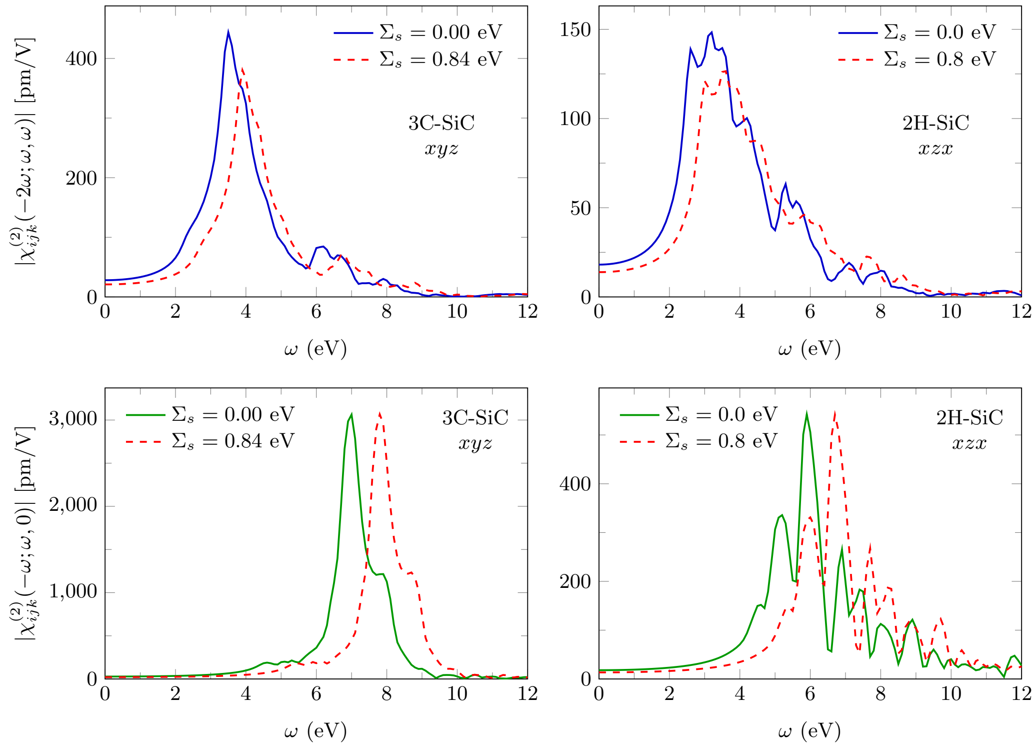

FIG. 2. Effect of the scissor on SHG and LEO susceptibilities, respectively, on the 1first and second row, applied on silicon carbide, cubic (3C-SiC) on the left side and hexagonal (2H-SiC) on the right. The dashed red curves include the scissor (QPA), while the solid ones do not (IPA).

and an ionic term and the ratio of these two contributions is referred to as the Faust-Henry coefficient $C^{\mathrm{FH}} = r^{S,i}/r^{S,e}$. Taking into account this relation between the electronic and ionic contributions gives the following expression for the electronic susceptibility $\chi^{(2),e}_{xyz}(-\omega;\omega,0)$ in terms of the full clamped LEO coefficient $r^{S}_{xyz}(\omega)$:

$$\chi^{(2),e}_{xyz}(-\omega;\omega,0) = -\frac{[\varepsilon(\omega)]^2\, r^{S}_{xyz}(\omega)}{2(1+C^{\mathrm{FH}})}, \tag{18}$$

where $\chi^{(2),e}$ and r^S are expressed in SI.

It allows for a comparison of our theoretical calculation with experimental clamped coefficients compiled by Adachi [30] from Refs. [31–39], for which we extracted the electronic part using Eq. (18). The Faust-Henry coefficient, $C^{\mathrm{FH}} = -0.51$ [33], has been measured at $\omega = 1$ eV and we have assumed it is constant in the energy range presented in Fig. 3 (red dots). We have also checked that if we take the ionic part as constant and given by its value at $\omega = 1$ eV, the results are very similar (blue crosses). One notes the dispersion between experimental values for a given frequency, as some of the clamped coefficients were estimated by Adachi from unclamped values. Nonetheless, we can see that we reach a rather good agreement on the electronic part within the QPA approximation, which lies in the range of the experimental data.

2. Gallium nitride

A few experimental studies were presented on a material similar to GaAs, that is, gallium nitride [40–42]. One of the main differences, however, between these two compounds is the width of their band gap, which, while it is a direct band gap in both cases, is much smaller for GaAs (~1.4 eV) than for GaN (~3.4 eV). Here we study its hexagonal polytype with a wurtzite structure, α-GaN. The first experimental studies were restricted to thin GaN layers, showing important divergences. It is only recently that high-quality materials, with a much larger thickness were studied, allowing for accurate comparison with theoretical calculations on bulk materials.

In Table II, we present the results for the electronic contribution $\chi^{(2)}$ in the independent-particle and quasiparticle approximation, showing the influence of the sScissors correction for this compound and GaAs for comparison. Using the set of Faust-Henry coefficients from Ref. [43], $C^{\mathrm{FH}}_x = -3.46$,

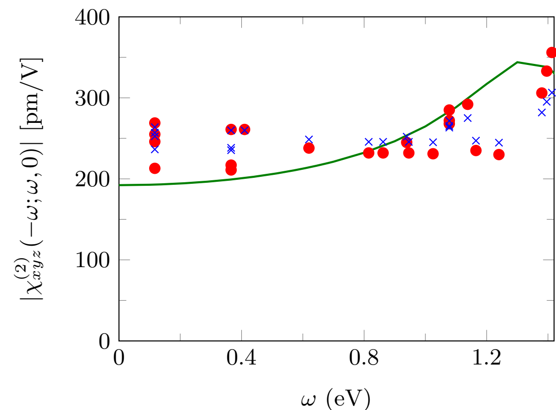

FIG. 3. Electronic part of the LEO susceptibility for GaAs calculated in this work (green curve) and extracted from the experimental results compiled in Ref. [30], with a constant Faust-Henry coefficient (red dots) or a constant ionic contribution (blue crosses).

TABLE II. Comparison with experimental values for excitation below the band gap of the purely electronic LEO susceptibility $\chi^{(2)}(-\omega;\omega,0)$ in pm/V for GaN. The values for GaAs are also given for comparison.

$\chi^{(2)}_{ijk}$	Expt. [42,44]	IPA	QPA
xxz (GaN)	5.0	6.3	4.6
zxx (GaN)	4.9	6.3	4.5
zzz (GaN)	7.9	13.7	9.0
xyz (GaAs)	200	455	193

$C_y^{\rm FH} = -3.81$, $C_z^{\rm FH} = -2.31$, we compare our values to the latest experimental results obtained by Irmer *et al.* [42]. Note that the components denoted d_{13}, d_{24}, and d_{33} in Ref. [42] correspond to half of $\chi^{(2)}_{xxz}$, $\chi^{(2)}_{zxx}$, and $\chi^{(2)}_{zzz}$, respectively.

Compared to GaAs, the effect of the scissors is relatively weak at low frequency: it always induces a decrease of the static value, but this decrease is only a few pm/V for GaN, while for GaAs it is close to 260 pm/V. This is linked to the fact that the spectrum of a large band-gap material, such as GaN, is quite flat in the low-energy range. On the contrary, for small band-gap material such as GaAs, the first series of peaks appears at low energy, leading to a fast increase of the susceptibility and a much larger effect of the scissors correction. However, we note that a better agreement with the experimental results can be obtained when the scissors correction is taken into account.

It is interesting to note that in this energy range, i.e., below the band gap, the knowledge of the Faust-Henry coefficients seems to be enough to account for the ionic motion.

3. Cubic silicon carbide

For zinc-blende symmetry, the dielectric tensor defined in Eq. (14) is diagonal, with $\varepsilon^{lr} = \varepsilon_{xx} = \varepsilon_{yy} = \varepsilon_{zz}$ and, as already stated in the previous section, $\chi^{(2)}_{xyz}$ is the only nonvanishing second-order component. By applying a dc field along the z-Cartesian axis, the dielectric tensor acquires an off-diagonal contribution:

$$\tilde{\varepsilon}_M^{(\mathcal{E}_z)}(\omega) = \begin{pmatrix} \varepsilon^{lr}(\omega) & \varepsilon^{\rm LEO}(\omega) & 0 \\ \varepsilon^{\rm LEO}(\omega) & \varepsilon^{lr}(\omega) & 0 \\ 0 & 0 & \varepsilon^{lr}(\omega) \end{pmatrix}, \qquad (19)$$

which can be expressed as $\varepsilon^{\rm LEO}(\omega) = 8\pi\chi^{(2)}_{xyz}(-\omega;\omega,0)\mathcal{E}_z$. In Figs. 4 and 5, we show the real and imaginary parts of the dielectric tensor and the induced component for 3C-SiC, calculated in the QPA. We chose a dc field with an amplitude of 10^6 V cm^{-1}, which corresponds to the value of the breakdown field for 3C-SiC [45]. It is the maximum strength of the field that can be used on a material before it breaks down and becomes electrically conductive and is most likely destroyed. The two components are displayed on different scales since the field-induced one is considerably smaller and would be indistinguishable otherwise, despite the fact that we used the most intense field possible. The static value of the real part of $\varepsilon^{\rm LEO}$ is small but nonzero. Since the field-induced component $\varepsilon^{\rm LEO}$ represents the extra-diagonal part of the tensor, its imaginary part, unlike the diagonal element, does not have to be greater than zero.

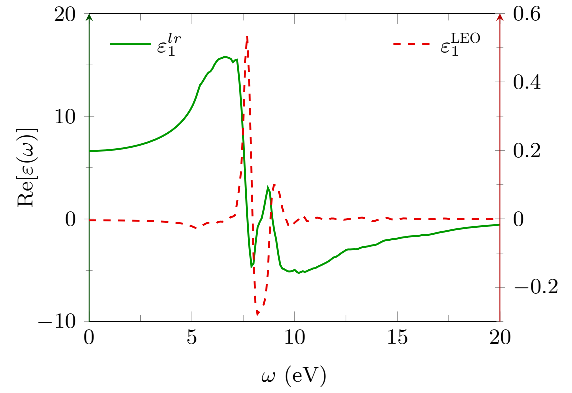

FIG. 4. Real part of the components of the dielectric tensor already present (solid green curve, scale on the left side) or induced by a static field (dashed red curve, scale on the right side) of 1.0×10^6 V cm^{-1} for cubic silicon carbide with a scissor of $\Sigma_s = 0.84$ eV.

The electronic part of the electro-optic coefficient $r^{S,e}_{xyz}(\omega)$, also noted $r^{S,e}_{41}$, is plotted in Fig. 6. The full clamped coefficient $r^S_{xyz}(\omega)$ is then plotted in the band-gap region, as obtained from the electronic susceptibility using Eq. (18). The Faust-Henry coefficient is given in Ref. [46], $C_x^{\rm FH} = 0.35$. The experimental value $r^S_{41}(\omega) = 2.7 \pm 0.5$ pm/V for $\omega = 2$ eV was reported in Ref. [47], while we find here $r^S_{41}(\omega) = 1.4$ pm/V for the QPA calculation. However, this calculation does not include local-field or excitonic effects. The influence of the local-field contribution has not yet been investigated for LEO but it has been for both the linear response and the second-harmonic generation. It was shown to be negligible for the linear response at $\omega = 2$ eV and reduces only slightly the value of the SHG susceptibility $\chi^{(2)}_{xyz}(-2\omega;\omega,\omega)$, from 38 to 33 pm/V. From these considerations, we have, for now, neglected the local fields and only included the excitonic effect using the α-kernel approximation to solve the Dyson equation defined in Eq. (12). It is a static approximation, depending on a single parameter α, independent of the frequency ω. However, two values are available for this parameter in the linear response. The static dielectric constant is well reproduced in TDDFT by using $\alpha = 0.3$, while $\alpha = 0.5$ gives a good absorption spectrum [20].

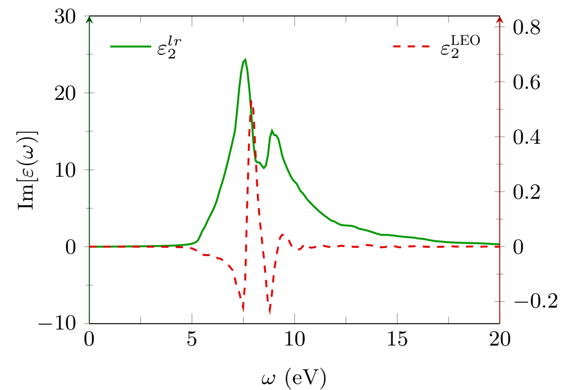

FIG. 5. Imaginary part of the components of the dielectric tensor already present (solid green curve, scale on the left side) or induced by a static field of 1.0×10^6 V cm^{-1} (dashed red curve, scale on the right side) for 3C-SiC.

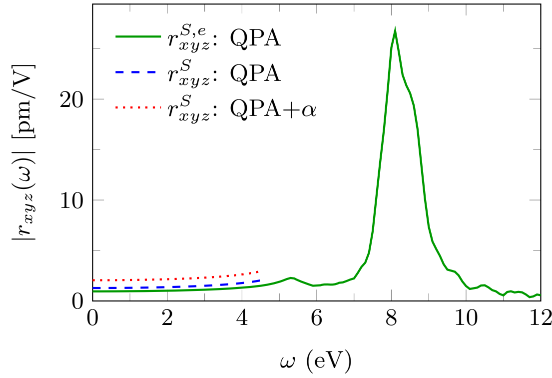

FIG. 6. Electro-optic coefficient of cubic silicon carbide (3C-SiC). Solid line (in green): electronic part of the QPA calculation. Dashed line (in blue): full clamped coefficient in QPA. Dotted line (in red): full clamped coefficient in the QPA plus α-kernel approximation with the static value $\alpha = 0.3$ and without local fields.

To compare with the experimental value measured for LEO at 2 eV, we expect that the static value of α should be used. The result of applying Eq. (12) is shown in Fig. 6 (red dotted curve) for the low-frequency region since the static value of α is used. As predicted, the amplitude of the spectrum is slightly increased. For comparison, we have also used $\alpha = 0.5$, increasing the LEO coefficients even further. It is also interesting to note that the effect of the α kernel on the LEO susceptibility is quite intricate: while the susceptibility is increased in the low-energy part of the spectrum, the amplitude of the absorption peak, not displayed here, is decreased. These effects are amplified when increasing the α parameter.

The value of the full clamped electro-optic coefficient at $\omega = 2$ eV is reported in Table III for different values of α. We conclude that by using a quasiparticle correction together with the α kernel, we reach a good agreement with the experimental point. However, due to the lack of other experimental data, it is not possible to get any conclusion on the best value for α.

B. Perpectives: Strained silicon

As previously stated, one way to generate a nonzero second-order susceptibility for silicon is to apply a strain on the material in order to break the centrosymmetry of the system. This kind of numerical calculation was done in Refs. [4,48] for second-harmonic generation and we have used here the same unit cells to simulate the strain inside the material, thus producing a LEO effect.

TABLE III. Effect of the value of α on the LEO susceptibility and electro-optic coefficient at $\omega = 2$ eV.

	α (a.u.)	$\chi^{(2)}_{xyz}$ (pm/V)	r^S_{41} (pm/V)
Expt. [47]			2.7 ± 0.5
QPA	0	24.8	1.37[1]
QPA+α_{static}	0.3	39.1	2.15[1]
QPA+α	0.5	55.2	2.40[1]

[1]These theoretical r^S_{41} coefficients were obtained using $C^{\text{FH}} = 0.35$ [46].

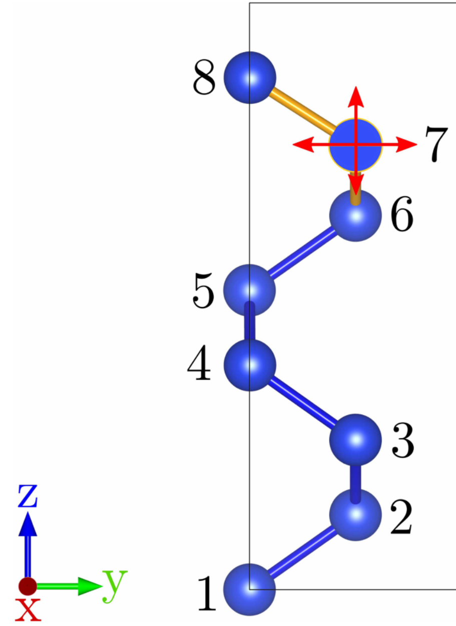

FIG. 7. Scheme of the strain applied inside the tetragonal unit cell: atom 7 is moved creating a compressive or tensile strain on the yellow bonds between atoms 6-7 and 7-8.

In the simulation, the strain is generated by moving atoms initially in their bulk positions, leading to an increase or a decrease of the bond lengths, therefore creating a tensile or compressive strain, respectively. In practice, the strain is applied on bulk Si, for which we switch from the diamondlike unit cell to the tetragonal cell shown in Fig. 7, where atom 7 is moved along the z axis for the uniaxial strain and in the (y,z) plane for the biaxial strain, generating an elongation or shortening of the bonds 6-7 and 7-8.

More details on the construction of the unit cells can be found in Ref. [48]. Moreover, the different structures are designated in a similar fashion, with the letters C and T used to refer to a compressive or tensile strain, respectively, with a percentage of elongation or compression of the bond compared to the bulk value. For instance, the structure $C_{1.8}_T_{3.0}$ refers to a compressive bond of 1.8% between atoms 6 and 7 and a tensile bond of 3.0% between atoms 7 and 8. The z coordinate of atoms 7 and 8 are given in Table IV for the structures $C_{1.8}_T_{3.0}$ and $C_{1.8}_C_{3.0}$. Note that, if the strain is the same in the two bonds, for instance $C_{3.0}_C_{3.0}$, then the pressure inside the material is not zero but the system is still centrosymmetric: the second-order susceptibility remains zero. If the strain in the two bonds is opposite, for instance $C_{3.0}_T_{3.0}$, then the pressure is compensated inside the material but $\chi^{(2)}$ is nonzero.

TABLE IV. Atomic positions: z coordinate for atoms 7 and 8 and lattice parameters.

	$C_{1.8}_T_{3.0}$	$C_{1.8}_C_{3.0}$	Relaxed bulk
Atom 7 (Å)	7.999	7.999	8.079
Atom 8 (Å)	9.478	9.214	9.425
a (Å)	3.81	3.81	3.81
c (Å)	10.82	10.56	10.77

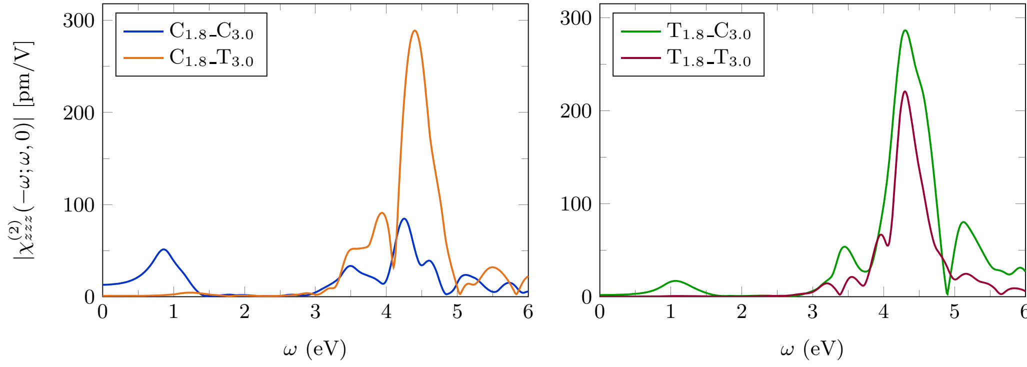

FIG. 8. Linear electro-optic spectra for uniaxial strained silicon in different configurations using a scissor $\Sigma_s = 0.6$ eV.

The spectra for different uniaxial strains are shown in Fig. 8. The band gap of the different systems is strongly decreased when the strain is applied: we get around 1 eV, using $\Sigma_s = 0.6$ eV, which is the scissors correction for bulk silicon [49]. Two structures appear in the spectra: the first one, around 1 eV, is situated in the gap of the unstrained bulk silicon and is ascribed to transitions between states induced by the strain. The second one around 4.4 eV is located at the position of the absorption peak in the linear response for bulk Si. For the second peak, the highest amplitude is reached for CT or TC strain, corresponding to a low pressure in the system. On the other hand, a compressive strain seems to be more efficient to generate the low-energy peak. Note also that the amplitude of the peak at low energy is always smaller than the one at higher energy.

The spectra for the biaxial strained system are displayed in Fig. 9. The letter Y is added to the denomination of the different systems to indicate an additional strain along the y axis. The component $\chi^{(2)}_{zzz}$ (in Fig. 9) obtained for the biaxial strain displays the same characteristics as for the uniaxial strain in Fig. 8, while the new nonzero component $\chi^{(2)}_{yyy}$, induced by the additional strain along Y, shows a much higher amplitude for the first peak around 1 eV. From that, we can conclude that a biaxial strain is more efficient to generate a high-intensity response in the band-gap region, whereas a uniaxial stress is enough if one is interested in the peak around 4.4 eV, corresponding to the position of the peak in the linear response spectrum of unstrained silicon.

a. *Comparison with experiments*. Although the way to apply the strain on the material is different, we can still have a general comparison with the LEO experiments in Ref. [3], where a compressive strain is applied by a straining layer deposited on top of silicon. An induced coefficient of 15 pm V^{-1} was found at $\omega = 0.8$ eV. It corresponds to what is found here for the $C_{0.7}$_$C_{3.0}$_Y system, which is at 11 pm V^{-1}.

b. *Comparison with SHG*. It was stressed in Ref. [48] that the uniaxial strain was more efficient in the low-energy range (around 1 eV) for SHG. It is shown in Fig. 8 that LEO has an opposite behavior, the peak situated at high energy being the most intense. We note that the effect of the strain configuration is roughly the same for the two processes, the C/C configuration being the most favorable for the low-energy part of the spectrum while the C/T or T/C cells will enhance the high-energy range. In the same way, for SHG and LEO, applying a biaxial strain is by far more efficient than a uniaxial strain to induce strong nonlinearities at low energy.

IV. CONCLUSION

In conclusion, in this work we have presented the derivation of the *ab initio* formalism developed for the calculation of the second-order susceptibility for the electro-optic effect. In our formalism, we have included the quasiparticle effect at the level of the scissors correction and the electron-hole interaction using a simplified scalar approach. On the other hand, we have not taken into account the local field effects, thus restricting us to the study of materials not presenting strong inhomogeneities.

We have applied our method to the calculation of LEO coefficients for the semiconductors GaAs, GaN, and SiC.

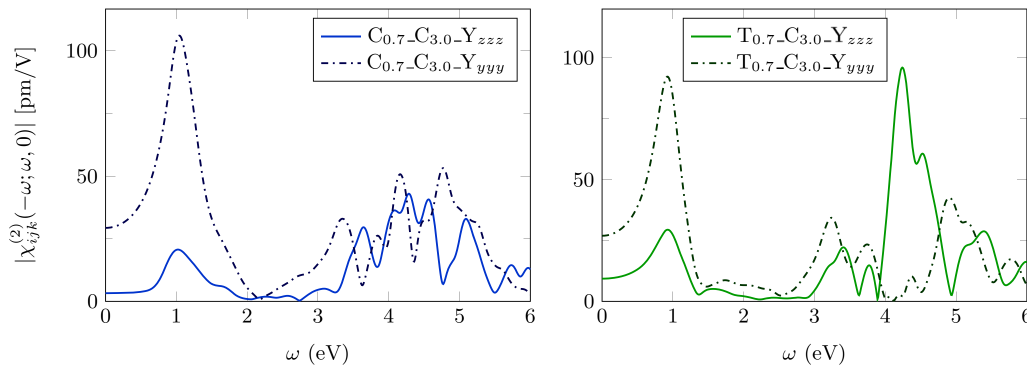

FIG. 9. Linear electro-optic spectra for biaxial strained Si with a scissor $\Sigma_s = 0.6$ eV. Solid line: component zzz; dot-dashed line: component yyy.

The ionic contribution has been included using Faust-Henry coefficients and we have compared our results with the experimental data presented in literature, finding a good agreement. Finally, we have also presented numerical values for strained silicon, showing that it is possible to induce large electro-optic susceptibilities.

This work shows that a high accuracy can be reached for the electronic part of the electro-optic coefficients for a large range of frequencies, opening the way to the investigation of more complex materials with technological interest.

ACKNOWLEDGMENTS

We are grateful for helpful discussions with E. Luppi and E. Degoli. This work was performed using HPC resources from GENCI-IDRIS Grant No. 090544.

[1] G. T. Reed, G. Mashanovich, F. Y. Gardes, and D. J. Thomson, Nat. Photonics **4**, 518 (2010).

[2] J. Frigerio, V. Vakarin, P. Chaisakul, M. Ferretto, D. Chrastina, X. Le Roux, L. Vivien, G. Isella, and D. Marris-Morini, Sci. Rep. **5**, 15398 (2015).

[3] R. S. Jacobsen, K. N. Andersen, P. I. Borel, J. Fage-Pedersen, L. H. Frandsen, O. Hansen, M. Kristensen, A. V. Lavrinenko, G. Moulin, H. Ou, C. Peucheret, B. Zsigri, and A. Bjarklev, Nature (London) **441**, 199 (2006).

[4] M. Cazzanelli, F. Bianco, E. Borga, G. Pucker, M. Ghulinyan, E. Degoli, E. Luppi, V. Véniard, S. Ossicini, D. Modotto, S. Wabnitz, R. Pierobon, and L. Pavesi, Nat. Mater. **11**, 148 (2012).

[5] Z. Cui, D. Liu, J. Miao, A. Yang, and J. Zhu, Phys. Rev. Lett. **118**, 043901 (2017).

[6] L. F. Lastras-Martínez, M. Chavira-Rodríguez, A. Lastras-Martínez, and R. E. Balderas-Navarro, Phys. Rev. B **66**, 075315 (2002).

[7] L. F. Lastras-Martínez, J. M. Flores-Camacho, A. Lastras-Martínez, R. E. Balderas-Navarro, and M. Cardona, Phys. Rev. Lett. **96**, 047402 (2006).

[8] E. Luppi and V. Véniard, Semicond. Sci. Technol. **31**, 123002 (2016).

[9] M. Veithen, X. Gonze, and P. Ghosez, Phys. Rev. B **71**, 125107 (2005).

[10] M. Veithen, First-principle study of the nonlinear responses of insulators to electric fields: Applications to ferroelectric oxides, Ph.D. thesis, Université de Liège, Belgium, 2005.

[11] J. L. P. Hughes and J. E. Sipe, Phys. Rev. B **53**, 10751 (1996).

[12] F. Nastos, B. Olejnik, K. Schwarz, and J. E. Sipe, Phys. Rev. B **72**, 045223 (2005).

[13] M. Veithen, X. Gonze, and P. Ghosez, Phys. Rev. Lett. **93**, 187401 (2004).

[14] T. R. Paudel and W. R. L. Lambrecht, Phys. Rev. B **79**, 245205 (2009).

[15] E. Luppi, H. Hübener, and V. Véniard, Phys. Rev. B **82**, 235201 (2010).

[16] This observation strongly depends on the way the formula is written considering that some two-band term can be recast as a sum of three- and two-band terms.

[17] G. Onida, L. Reining, and A. Rubio, Rev. Mod. Phys. **74**, 601 (2002).

[18] H. Hübener, Second harmonic generation in solids: Theory and simulation, Ph.D. thesis, Ecole Polytechnique, 2010.

[19] L. Reining, V. Olevano, A. Rubio, and G. Onida, Phys. Rev. Lett. **88**, 066404 (2002).

[20] S. Botti, F. Sottile, N. Vast, V. Olevano, L. Reining, H.-C. Weissker, A. Rubio, G. Onida, R. Del Sole, and R. W. Godby, Phys. Rev. B **69**, 155112 (2004).

[21] The ABINIT code is a common project of the Université Catholique de Louvain, Corning Incorporated, and other contributors (http://www.abinit.org).

[22] X. Gonze, F. Jollet, F. A. Araujo, D. Adams, B. Amadon, T. Applencourt, C. Audouze, J.-M. Beuken, J. Bieder, A. Bokhanchuk, E. Bousquet, F. Bruneval, D. Caliste, M. Côté, F. Dahm, F. D. Pieve, M. Delaveau, M. D. Gennaro, B. Dorado, C. Espejo, G. Geneste, L. Genovese, A. Gerossier, M. Giantomassi, Y. Gillet, D. Hamann, L. He, G. Jomard, J. L. Janssen, S. L. Roux, A. Levitt, A. Lherbier, F. Liu, I. Lukacevic, A. Martin, C. Martins, M. Oliveira, S. Poncé, Y. Pouillon, T. Rangel, G.-M. Rignanese, A. Romero, B. Rousseau, O. Rubel, A. Shukri, M. Stankovski, M. Torrent, M. V. Setten, B. V. troeye, M. Verstraete, D. Waroquier, J. Wiktor, B. Xue, A. Zhou, and J. Zwanziger, Comput. Phys. Commun. **205**, 106 (2016).

[23] X. Gonze, B. Amadon, P.-M. Anglade, J.-M. Beuken, F. Bottin, P. Boulanger, F. Bruneval, D. Caliste, R. Caracas, M. Côté, T. Deutsch, L. Genovese, P. Ghosez, M. Giantomassi, S. Goedecker, D. Hamann, P. Hermet, F. Jollet, G. Jomard, S. Leroux, M. Mancini, S. Mazevet, M. Oliveira, G. Onida, Y. Pouillon, T. Rangel, G.-M. Rignanese, D. Sangalli, R. Shaltaf, M. Torrent, M. Verstraete, G. Zerah, and J. Zwanziger, Comput. Phys. Commun. **180**, 2582 (2009).

[24] X. Gonze, G.-M. Rignanese, M. Verstraete, J.-M. Beuken, Y. Pouillon, R. Caracas, F. Jollet, M. Torrent, G. Zerah, M. Mikami, Ph. Ghosez, M. Veithen, J.-Y. Raty, V. Olevano, F. Bruneval, L. Reining, R. Godby, G. Onida, D. R. Hamann, and D. C. Allan, Z. Kristallogr. **220**, 558 (2005).

[25] E. Luppi, H. Hübener, and V. Véniard (unpublished).

[26] S. M. Anderson, N. Tancogne-Dejean, B. S. Mendoza, and V. Véniard, Phys. Rev. B **91**, 075302 (2015).

[27] C. Attaccalite and M. Grüning, Phys. Rev. B **88**, 235113 (2013).

[28] M. Grüning and C. Attaccalite, Phys. Rev. B **89**, 081102 (2014).

[29] S. H. Wemple and D. DiDomenico, *Applied Solid State Science*, edited by R. Wolfe (Academic Press, New York, 1972), Vol. 3, p. 263.

[30] S. Adachi, *GaAs and Related Materials: Bulk Semiconducting and Superlattice Properties* (World Scientific, Teaneck, NJ, 1994).

[31] C.-A. Berseth, C. Wuethrich, and F. K. Reinhart, J. Appl. Phys. **71**, 2821 (1992).

[32] Y. V. Shaldin and D. A. Belogurov, Sov. J. Quantum Electron. **6**, 897 (1976).
[33] N. Suzuki and K. Tada, Jpn. J. Appl. Phys. **23**, 1011 (1984).
[34] J. Faist and F. Reinhart, J. Appl. Phys. **67**, 6998 (1990).
[35] M. Sugie and K. Tada, Jpn. J. Appl. Phys. **15**, 421 (1976).
[36] A. Yariv, C. Mead, and J. Parker, IEEE J. Quantum Electron. **2**, 243 (1966).
[37] W. D. Johnston and I. P. Kaminow, Phys. Rev. **188**, 1209 (1969).
[38] I. Kaminow, IEEE J. Quantum Electron. **4**, 23 (1968).
[39] G. L. Herrit and H. E. Reedy, MRS Proceedings **152**, 169 (1989).
[40] X.-C. Long, R. A. Myers, S. R. J. Brueck, R. Ramer, K. Zheng, and S. D. Hersee, Appl. Phys. Lett. **67**, 1349 (1995).
[41] S. Shokhovets, R. Goldhahn, and G. Gobsch, Mater. Sci. Eng.: B **93**, 215 (2002).
[42] G. Irmer, C. Roder, C. Himcinschi, and J. Kortus, Phys. Rev. B **94**, 195201 (2016).
[43] G. Irmer, C. Roder, C. Himcinschi, and J. Kortus, J. Appl. Phys. **116**, 245702 (2014).
[44] S. Bergfeld and W. Daum, Phys. Rev. Lett. **90**, 036801 (2003).
[45] Y. Goldberg, M. Levinshtein, and S. Rumyantsev, *Properties of Advanced Semiconductor Materials GaN, AlN, SiC, BN, SiC, SiGe*, edited by M. E. Levinshtein, S. L. Rumyantsev, and M. S. Shur (Wiley, New York, 2001), pp. 93–148.
[46] G. L. Harris, *Properties of Silicon Carbide* (IET, Stevenage, 1995).
[47] X. Tang, K. G. Irvine, D. Zhang, and M. G. Spencer, Appl. Phys. Lett. **59**, 1938 (1991).
[48] E. Luppi, E. Degoli, M. Bertocchi, S. Ossicini, and V. Véniard, Phys. Rev. B **92**, 075204 (2015).
[49] T. Cheiwchanchamnangij and W. R. L. Lambrecht, Phys. Rev. B **84**, 035203 (2011).